REPORT DOCUMENTATION PAGE

Form Approved

OMB No. 0704-0188

1. REPORT DATE *(DD-MM-YYYY)*	2. REPORT TYPE	3. DATES COVERED *(From - To)*
10-Aug-2015	Final	14 Jun 2015 to 13 Jun 2015

4. TITLE AND SUBTITLE

Exploring Novel Spintronic Responses from Advanced Functional Organic Materials

5a. CONTRACT NUMBER
FA2386-12-1-4008

5b. GRANT NUMBER
Grant AOARD-124008

5c. PROGRAM ELEMENT NUMBER
61102F

6. AUTHOR(S)

Prof. Soo Young Park

5d. PROJECT NUMBER

5e. TASK NUMBER

5f. WORK UNIT NUMBER

7. PERFORMING ORGANIZATION NAME(S) AND ADDRESS(ES)

Seoul National University
1 Gwanak-Ro
Kwanak-gu, Seoul 151-744
Korea (South)

8. PERFORMING ORGANIZATION REPORT NUMBER

N/A

9. SPONSORING/MONITORING AGENCY NAME(S) AND ADDRESS(ES)

AOARD
UNIT 45002
APO AP 96338-5002

10. SPONSOR/MONITOR'S ACRONYM(S)

AFRL/AFOSR/IOA(AOARD)

11. SPONSOR/MONITOR'S REPORT NUMBER(S)

AOARD-124008

12. DISTRIBUTION/AVAILABILITY STATEMENT

Distribution A: Approved for public release. Distribution

13. SUPPLEMENTARY NOTES

14. ABSTRACT

In this project, we investigated magnetic property of π-conjugated molecules and application of spin-radical containing molecule. This report has three parts. First, we will report the results of organic magnetoresistance (OMAR) in field effect transistors. We observed OMAR in ambipolar field effect transistors based on Hex-4-TFPTA. Underlying mechanism of OMAR was tuned by changing source-drain voltage from positive (+100 V) to negative (-100 V) at fixed gate voltage (+100V). The maximum MR values were +3% and +0.4% at 100 mT, respectively. We conclude that dominant OMAR mechanism can be changed by injecting minority charge carriers. Second, we will report on the spin-radical containing fluorescent organic molecule for ascorbic acid (AA) sensor. A novel nitronyl-nitroxide derivative (NN-CN-TFFP) for highly sensitive and selective detection of AA operating over broad concentration range from 1 μM to 2 mM is reported. The probe showed 260-fold fluorescence turn-on and diminished electron spin resonance (ESR) signal upon AA addition. Finally, we will briefly report the result of collaboration work with Prof. Bin Hu group has characterized optically tunable Seebeck effect from the intramolecular proton-transfer materials originally synthesized in our group.

15. SUBJECT TERMS

organic magnetoresistance, OMAR, Ascorbic acid sensor

16. SECURITY CLASSIFICATION OF:			17. LIMITATION OF ABSTRACT	18. NUMBER OF PAGES	19a. NAME OF RESPONSIBLE PERSON
a. REPORT	b. ABSTRACT	c. THIS PAGE			Misoon Y. Mah, Ph.D.
U	U	U	SAR	30	19b. TELEPHONE NUMBER *(Include area code)* +81-3-5410-4409

Final Report for AOARD Grant #FA2386-12-1-4008

Exploring Novel Spintronic Responses from Advanced Functional Organic Materials

08. 10. 2015

Jin Hong Kim, Soo Young Park

Name of Principal Investigators (PI and Co-PIs): Soo Young Park

E-mail: parksy@snu.ac.kr
Institution: Seoul National University
Mailing Address: 1 Gwanak-ro, Gwanak-gu, Seoul 151-744, Korea
Phone: +82-2-880-8327
Fax: +82-2-886-8331

Period of Performance: 14 Jun. 2012 – 13 Jun. 2015

Abstract

This AOARD joint project (#FA2386-12-1-4008) originally aimed to explore novel spintronic responses from advanced functional organic materials comprising π-conjugated molecules. For collaboration works, various kinds of organic materials prepared in our group were supplied to Bin Hu and Andre Persoons groups. In addition to such materials supply activity, we also tried to investigate magnetic property of our own materials and to develop new applications by ourselves.

This report has three parts. First, we will discuss organic magnetoresistance (OMAR) in the field effect transistors. We observed OMAR in ambipolar field effect transistors based on Hex-4-TFPTA. Underlying mechanism of OMAR was tuned by changing source-drain voltage from positive (+100 V) to negative (-100 V) at fixed gate voltage (+100V). The maximum MR values were +3% and +0.4% at 100 mT, respectively. We also observed that MR was dependent on V_G and temperature. It was found that the dominant mechanism of magnetoresistance could be changed by the minority charge carrier injection. Second, we will report on the spin-radical containing fluorescent organic molecule for ascorbic acid (AA) sensor. A novel nitronyl-nitroxide derivative (NN-CN-TFFP) for highly sensitive and selective detection of AA operating over broad concentration range from 1 μM to 2 mM has been developed in this work. The probe showed 260-fold fluorescence turn-on and diminished electron spin resonance (ESR) signal upon AA addition. Finally, we will briefly report the result of collaboration work with Prof. Bin Hu group has characterized optically tunable Seebeck effect from the intramolecular proton-transfer materials originally synthesized in our group.

Contents

Chapter 1. Organic magnetoresistance

1.1. Introduction

Since the first observation in 2003,[1] organic magnetoresistance (OMAR) has been attracting much more attention due to their potential application to cheap plastic organic magnetic sensor[2] as well as their interesting phenomena from a physical point of view.[3] OMAR refers to the resistance (or current) changes in organic device under magnetic field of a few millitesla without ferromagnetic electrode. Magnetoresistance (MR) is evaluated as MR = $\Delta R(B)/R(0)=[\{R(B)-R(0)\}/R(0)]$ where R(B) and R(0) are resistance with and without magnetic field (B), respectively. It is believed that the origin of OMAR is highly related to the hyperfine field of hydrogen atoms which affects various spin interactions between the spin carrying quasiparticles.[4] However, the specific mechanism between those particles is still debated. There are three representative models to explain this phenomenon: bipolaron,[5] electron-hole pairs (e-h pairs)[6] and triplet exciton-polaron interaction (TPI) models (**Figure 1.1**).[7] The bipolaron model is based on the interaction between same kinds of charge carriers (single carrier model) while the others are based on interactions between the opposite sign charge carriers (double carrier model). Recent studies revealed that more than two mechanisms could be involved in a single device depending on the sample preparation and measuring condition.[8, 9] For a deeper understanding of OMAR and developing new organic devices, controlling dominant underlying mechanism by simple method should be explored in advance.

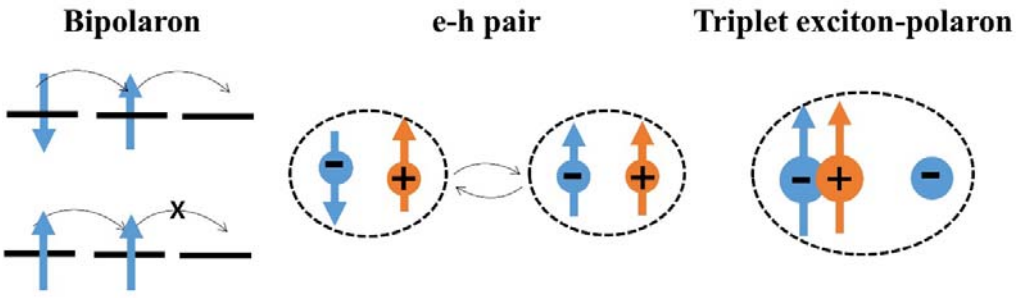

Figure 1.1. Schematic illustration of the particle interactions based on three representative OMAR models. If the bipolarons are generated as intermediate state, charge transport can be blockaded depending on the spins of the two particles (triplet bipolaron are forbidden). In the

e-h pair model, B changes the singlet to triplet e-h pair ratio. Due to different recombination/dissociation of singlet and triplet e-h pairs, B dependent recombination/dissociation can occur. In TPI model, B change the number of triplet exciton or triplet-charge reaction rate. Triplet exciton-charge interaction can contribute current by detrapping charge or scattering charge.

In order to modulate mechanism, several experimental strategies based on two-terminal devices have been commonly investigated. In most cases, tuning the mechanism could be achieved by controlling fabrication condition such as charge blocking layer thickness, material blending ratio and surface treatment, which can restrict flexibility in developing applications [8, 10, 11]. On the other hand, organic field effect transistors (OFETs) provide distinct advantage due to their capability of manipulating sign and density of charge carriers. Particularly, in ambipolar OFETs, it is possible to change from unipolar to bipolar regime by adjusting gate voltage (V_G) and drain-source voltage (V_{DS}), which is suitable for investigating both single and double carrier model of MR in a single device.[12] However, only a handful of materials have been investigated in transistor structure until now. Reichert and Saragi reported photo-induced MR in acene materials and also bipolaron model related MR in spirobifluorene derivatives.[13, 14] Pham et al. demonstrated e-h pair model based MR in donor-acceptor bilayer transistors.[15] Although mechanism change (between bipolaron and e-h pair model) was reported in some cases including these examples under light illumination condition, there is no example of mechanism control in the dark condition for the OFET device.

In the present work, we report OMAR in *n*-channel dominant ambipolar OFETs based on (2E,2'E)-3,3'-(2,5-dihexyloxy-1,4-phenylene)bis(2-(5-(4-(trifluoromethyl)phenyl)thiophen-2-yl)acrylonitrile) (Hex-4-TFPTA). We could successfully tune underlying mechanism though applying different sign of V_{DS} at fixed V_G of 100 V in the dark. MR values reached +3 % at V_{DS} = +100 V and +0.4 % at V_{DS} = -100 V under 100 mT of magnetic field, respectively. Based on the V_G and temperature dependent MR results, it was deduced that the double charge

carrier models are dominant in the V_{DS} = +100 V condition while single charge carrier model, i.e. bipolaron model, is expected to work in the V_{DS} = -100 V.

1.2. Experimental

Materials: Hex-4-TFPTA was synthesized as shown in **Scheme 1.1,** and then was purified by sublimation. Detailed synthetic methods were reported in our previous paper [16].

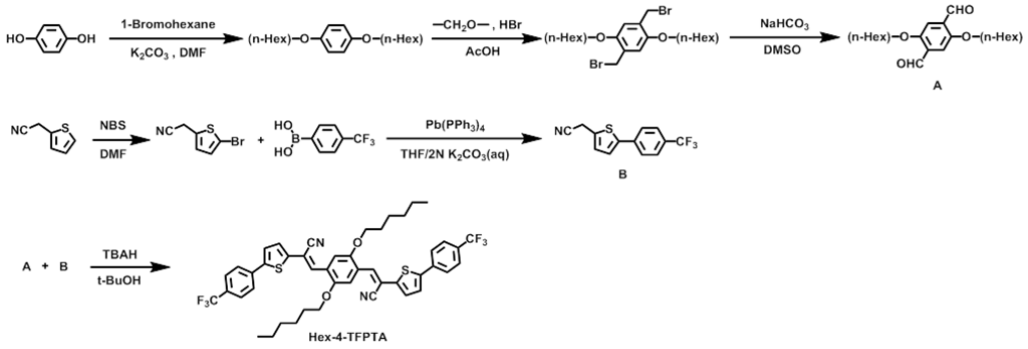

Scheme 1.1. Synthetic route of Hex-4-TFPTA

Device fabrication & measurement: SiO_2/Si (300 nm-thick SiO_2 with gold source-drain electrode on top for bottom contact devices) substrates were cleaned by sonication in acetone and isopropyl alcohol. The substrates were then exposed to UV (360 nm) for 20 min, and the octadecyltrichlorosilane (OTS) treatment was carried out in an OTS vapor chamber (80 °C, vacuum, 2 h 30 min). Then 30 nm of Hex-4-TFPTA was thermally deposited in a vacuum chamber (**Figure 1.2**). The current was measured by a Keithley 6517A electrometer. During the measurement, magnetic field was switched on and off at 3 s intervals. All measurements were conducted in a vacuum chamber at room temperature except for temperature dependent measurements.

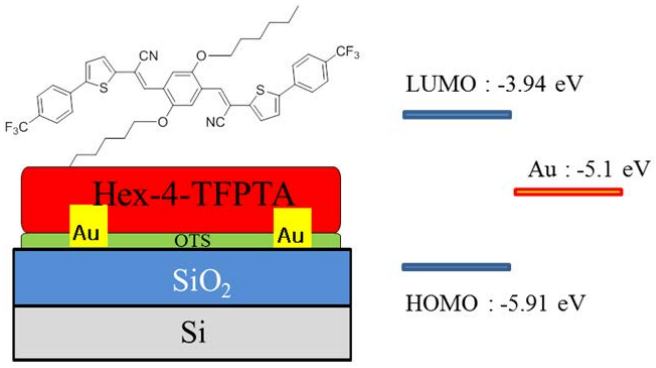

Figure 1.2. Structure of a bottom-contact OFET device and energy level diagrams of Hex-4-TFPTA and gold.

1.3. Results and Discussion

In the previous paper, we have characterized Hex-4-TFPTA as a unipolar *n*-channel material for OFETs.[16] Recently, we also found that new batch of Hex-4-TPFTA exhibited *n*-channel dominant ambipolar characteristics in the high electric field condition. Considering the work function of gold (-5.1 eV) and HOMO energy level of Hex-4-TFPTA (-5.91 eV), it is acceptable that hole can be injected from gold electrode to Hex-4-TFPTA film under high electric field. Because OFETs property is influenced by impurities, this minority carrier (hole) injection could be attributed to the higher purification level of new batch than that of previous one. **Figures 1.3a-d** show the transfer and output curves of Hex-4-TFPTA field-effect transistors. The electron mobility (μ_e) of 2×10^{-2} cm^2/Vs was calculated in the saturation region (V_{DS} = 100 V). Compared to the previously reported value which was measured at top-contacted devices (average μ_e : 1.56 cm^2/Vs), bottom-contacted devices explored in this work exhibited lower electron mobility. From the S-shaped *n*-channel output curve at low V_{DS}, it is noted that such low mobility is derived from the injection problems of bottom-contacted geometry (**Figure 1.2b**). In contrast to the typical *n*-channel property, *p*-channel property of Hex-4-TFPTA was very week. V-shape of both *n*- and *p*- channel transfer curve and current incensement of *n*-channel output curve at high V_{DS} explained that hole injection occurred at high field condition (**Figures 1.2a-c**). But we could not observe saturated *p*-channel output curve from our measurement system (**Figure 1.2d**). Thus, it is expected that although hole

could be injected from electrode, it could not accumulate or transport along the full channel area. In other word, most of injected hole remained as immobile state near the electrode.

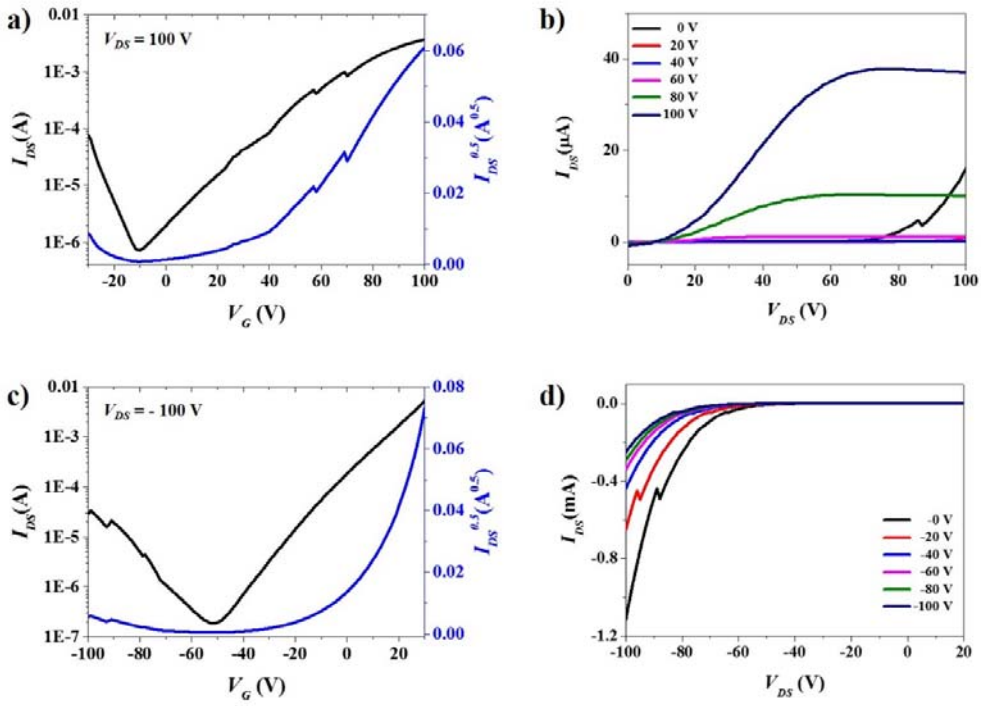

Figure 1.3. Transfer and output characteristics of OFET device based on thin film of Hex-4-TFPTA. **a), b)** for *n*-channel and **c), d)** for *p*-channel respectively.

Based on these devices, we conducted MR measurement at constant V_G of +100 V. **Figures 1.4a,c** show the current change under different magnetic field while applying V_{DS} = +100 V and -100 V, respectively. **Figures 1.4b,d** depict corresponding MR curves. Although current levels were similar to each other, the MR values were different; 3% at V_{DS} = +100 V and 0.4% at V_{DS} = -100 V under 100 mT of magnetic field. The main differences between two conditions are the densities of accumulated electron and injected hole. Accumulated charge density at certain position (x) is related to effective gate voltage (V_{eff}(x)) which is defined as the difference between the applied V_G and the channel potential (V(x)).[12] At V_G = +100 V and V_{DS} = +100 V, electrons were injected and accumulated from source electrode to pinch-off point

where V_{eff} was equal to the threshold voltage (V_{th}), while holes were injected from drain electrode. On the other hand, because high positive V_{eff} was applied along the whole channel, accumulating electron without pinch off point, hole injection could be restricted at V_{DS} = -100 V. Therefore, the origin of the higher MR value at V_{DS} = +100 V than that of at V_{DS} = -100 V could be attributed to hole injection related double charge carrier model of MR.

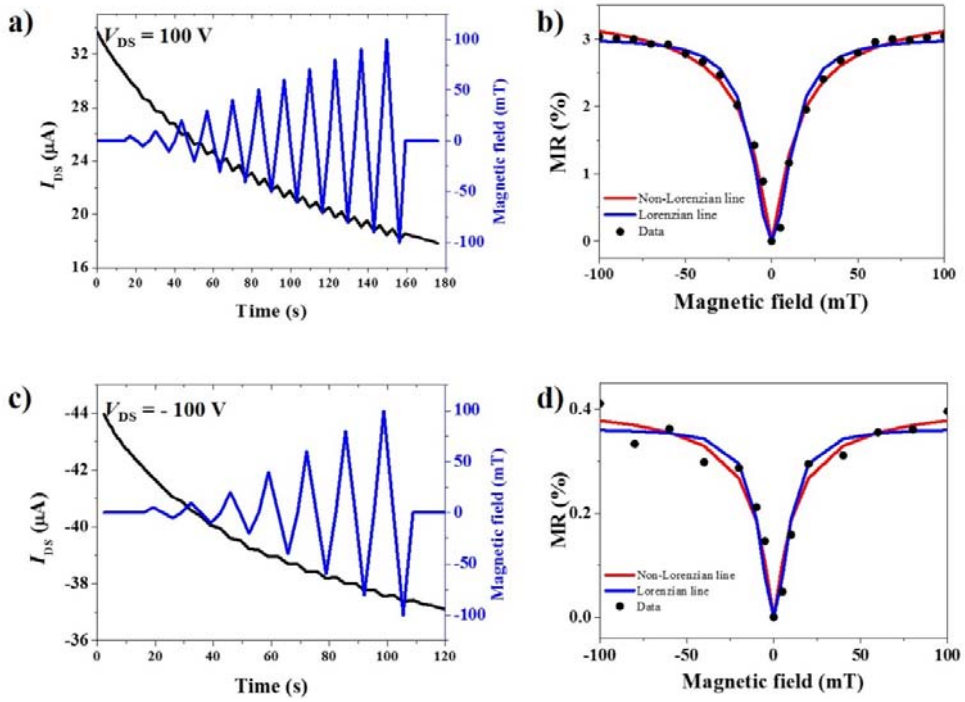

Figure 1.4. a, c) Magnetic field effect on the current at different V_{DS} and **b, d)** the corresponding MR curve of Hex-4-TFPTA thin film transistor.

In order to verify hole injection effect on MR, we carried out V_G dependent MR measurement. **Figure 1.5a** shows that MR value was increased with increasing V_G. Because injected holes are expected to be immobile near the electrode, electron pinch off position is important to interaction between electron and hole. When the V_G was increased at fixed V_{DS}, more electrons were accumulated along the channel and the pinch off position would be moved to the drain electrode. Thus more interaction between electron and hole was expected at higher V_G. **Figure 1.5b** supports this assumption. The

electro-luminescence (EL) intensity, which originates from the hole and electron recombination, was increased when the applied V_G has increased over 40V at V_{DS} = 100V. Accordingly, there was large gap in MR value between V_G = 40 V and V_G = 60 V (**Figure 1.5a**), which implied that minority charge carrier injection and consequent electron-hole interaction played an important role in MR tuning.

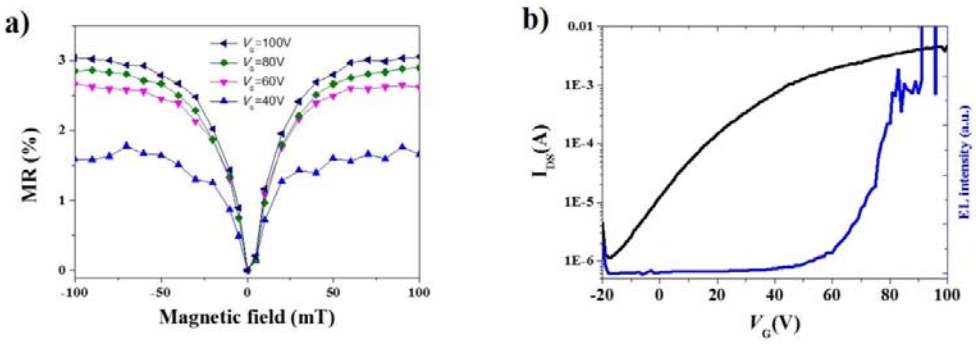

Figure 1.5. a) V_G dependent MR value at V_{DS} = 100V, b) I_{DS} and corresponding EL intensity at V_{DS} = 100V.

Temperature dependent MR measurement was undertaken to obtain further information of both V_{DS} conditions. In the V_{DS} = +100 V condition, the MR was increased with increasing temperature from 100 K to 300 K (**Figure 1.6a**). Because only small amount of hole charge carriers are expected compared to electron charge carriers, hole injection might be important to form excited state and MR. Although injection mechanism at metal-organic interface is still unclear, most of theories are based on classical thermal-field emission model where sufficient thermal energy is necessary to overcome the energy barrier height.[17] Thus abruptly enhanced MR between 200 K and 300 K can be attributed to sufficient hole injection by enough thermal energy. On the other hand, different result was observed in V_{DS} = -100 V condition. MR value at high temperatures was lower than that at 100 K as depicted **Figure 1.6b.** Recently, Isenberg et al. reported that trapped charges between organic semiconductors and dielectric layer are important to bipolaron based OMAR in OFETs.[13] It has been also reported that trapped charge carriers can cause spin blockades.[18] Based on charge hopping model, trapped charge carriers density is high at low temperature. Thus, we could expect that single charge carrier model based OMAR was dominant in this restricted hole injection condition.

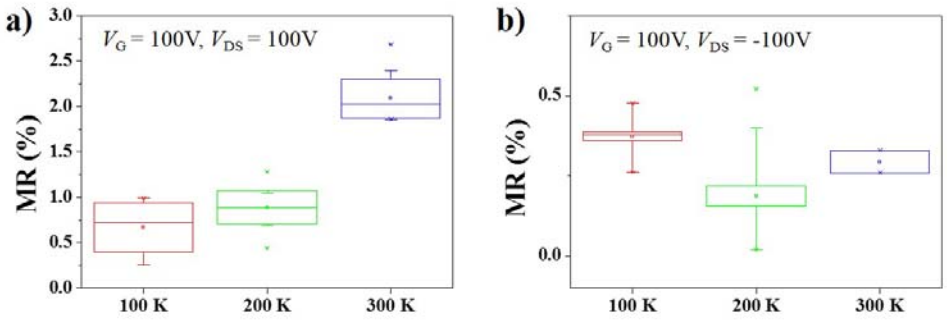

Figure 1.6. a,b) Temperature dependent MR value.

In the following, we will briefly suggest possible explanation for positive MR in double charge carrier condition. When electron and hole carriers are collided, they could form singlet and triplet e-h pairs with a ratio of 1:3. E-h pairs could recombine to excitons or dissociate to free charge carriers. Singlet and triplet e-h pairs could be mixed by the hyperfine fields until applying external magnetic field. When the magnetic field suppresses this spin mixing, singlet to triplet excitons ratio can be changed [6, 10, 19]. Both e-h pair and TPI model can contribute to current.[19] By assuming faster singlet exciton

formation rate than triplet exciton, applying magnetic field can decrease singlet to triplet excited state ratio. Because singlet state e-h pair has large dissociation rate than triplet one,[20] decreased singlet to triplet ratio can contribute to less dissociated secondary charge carrier (+MR).[19] In TPI model, because triplet exciton has longer lifetime than singlet exciton, enhanced triplet exciton portion can hinder the charge transport by scattering charge carriers (+MR).[10, 19]

In conclusion, we could demonstrate dark state MR from 0.4 % to 3 % by alternating applied V_{DS} sign in ambipolar OFETs based on Hex-4-TFPTA. In positive V_{DS} condition, MR was depended on V_G and temperature indicating double charge carrier model is dominant mechanism. On the other hand, in negative V_{DS} region, unipolar charge transport condition, single charge carrier model based OMAR is most likely operating.

Acknowledgement

Note that we performed this research with Tada group in Osaka University (Japan).

1.4. References

[1] J. Kalinowski, M. Cocchi, D. Virgili, P. Di Marco, V. Fattori, Chemical Physics Letters 2003, 380, 710.

[2] W. J. Baker, K. Ambal, D. P. Waters, R. Baarda, H. Morishita, K. van Schooten, D. R. McCamey, J. M. Lupton, C. Boehme, Nature communications 2012, 3, 898.

[3] T. L. Francis, O. Mermer, G. Veeraraghavan, M. Wohlgenannt, New Journal of Physics 2004, 6, 185; Ö. Mermer, G. Veeraraghavan, T. L. Francis, Y. Sheng, D. T. Nguyen, M. Wohlgenannt, A. Köhler, M. K. Al-Suti, M. S. Khan, Physical Review B 2005, 72.

[4] T. D. Nguyen, G. Hukic-Markosian, F. Wang, L. Wojcik, X.-G. Li, E. Ehrenfreund, Z. V. Vardeny, Nat Mater 2010, 9, 345.

[5] W. Wagemans, F. L. Bloom, P. A. Bobbert, M. Wohlgenannt, B. Koopmans, Journal of Applied Physics 2008, 103; P. A. Bobbert, T. D. Nguyen, F. W. A. van Oost, B. Koopmans, M. Wohlgenannt, Physical Review Letters 2007, 99, 216801.

[6] V. N. Prigodin, J. D. Bergeson, D. M. Lincoln, A. J. Epstein, Synthetic Metals 2006, 156,

757.

[7] P. Desai, P. Shakya, T. Kreouzis, W. P. Gillin, N. A. Morley, M. R. J. Gibbs, Physical Review B 2007, 75, 094423; P. Desai, P. Shakya, T. Kreouzis, W. P. Gillin, Physical Review B 2007, 76, 235202.

[8] P. Janssen, M. Cox, S. H. W. Wouters, M. Kemerink, M. M. Wienk, B. Koopmans, Nature communications 2013, 4.

[9] T. Omori, Y. Wakikawa, T. Miura, Y. Yamaguchi, K.-i. Nakayama, T. Ikoma, The Journal of Physical Chemistry C 2014, 118, 28418; M. Fayolle, M. Yamaguchi, T. Ohto, H. Tada, Journal of Applied Physics 2015, 117, 075501.

[10] B. Hu, Y. Wu, Nat Mater 2007, 6, 985.

[11] H.-J. Jang, S. J. Pookpanratana, A. N. Brigeman, R. J. Kline, J. I. Basham, D. J. Gundlach, C. A. Hacker, O. A. Kirillov, O. D. Jurchescu, C. A. Richter, ACS Nano 2014, 8, 7192.

[12] M. S. Kang, C. D. Frisbie, Chemphyschem 2013, 14, 1547; E. C. P. Smits, T. D. Anthopoulos, S. Setayesh, E. van Veenendaal, R. Coehoorn, P. W. M. Blom, B. de Boer, D. M. de Leeuw, Physical Review B 2006, 73.

[13] C. Isenberg, T. P. I. Saragi, Journal of Materials Chemistry C 2014, 2, 8569.

[14] E. Tatarov, T. Reichert, T. P. I. Saragi, A. Scheffler, R. Ueberschaer, C. Bruhn, T. Fuhrmann-Lieker, J. Salbeck, Chemical Communications 2013, 49, 4564; T. P. I. Saragi, T. Reichert, Applied Physics Letters 2012, 100, 073304; T. Reichert, T. P. I. Saragi, J. Salbeck, RSC Advances 2012, 2, 7388; T. Reichert, T. P. I. Saragi, Organic Electronics 2012, 13, 377; T. Reichert, T. P. I. Saragi, Applied Physics Letters 2011, 98, 063307.

[15] S.-T. Pham, Y. Kawasugi, H. Tada, Applied Physics Letters 2013, 103.

[16] S. W. Yun, J. H. Kim, S. Shin, H. Yang, B.-K. An, L. Yang, S. Y. Park, Advanced Materials 2012, 24, 911.

[17] T. N. Ng, W. R. Silveira, J. A. Marohn, Physical Review Letters 2007, 98; Y. Kimura, T. Oba, N. Shimakura, M. Niwano, Applied Physics Letters 2009, 94, 073303.

[18] N. J. Harmon, M. E. Flatté, Journal of Applied Physics 2014, 116.

[19] B. Hu, L. Yan, M. Shao, Advanced Materials 2009, 21, 1500.

[20] M. Wohlgenannt, Z. V. Vardeny, Journal of Physics: Condensed Matter 2003, 15, R83; J. Kalinowski, J. Szmytkowski, W. Stampor, Chemical Physics Letters 2003, 378, 380.

Chapter 2. Novel stable nitroxide radical-bearing π-conjugated organic materials

2.1. Introduction

Ascorbic acid (AA), also known as Vitamin C, is a naturally occurring antioxidant and plays important roles in many biological processes in human body such as a cofactor in enzymatic reactions, collagen synthesis, scurvy prevention, and immune system enhancement.[1-3] It has also been widely used as a food additive to prevent oxidation in juices and soft drinks.[4, 5] Moreover, it has been reported that AA has a positive effect on cancer therapy.[6] Accordingly, there is ever increasing interest in AA detection where its concentration varies from 5 μM in human blood plasma and serum to 20 mM in food and pharmaceuticals.[5-7] A lot of analytical detection methods for AA have been developed including electrophoresis,[8] UV-Vis absorption spectroscopy,[9, 10] liquid chromatography,[4, 11] and electrochemistry,[5, 12, 13] so far. In recent years, fluorescence-based method has become a popular approach for AA detection because it offers many advantages over other methods in terms of the sensitivity, convenience, and non-invasiveness.[14] A number of fluorescent probes for AA have been reported utilizing redox reactions with $KMnO_4$,[15] MnO_2 nanosheets,[16] chromium(VI) ions,[17] Au nanoclusters (AuNCs),[18] silver nanoparticles,[19] DNA,[20] electrochromic dyes,[21] and nitroxides.[22-34] These studies greatly advanced the research on the fluorescence detection of AA; however, many of these probes suffer from relatively low sensitivity and narrow detection range due to the inefficiency of the AA-reactive fluorescence quenching group. Therefore, particularly considering a wide variety of AA concentration in different analytic samples, new AA probes possessing broad detection range as well as high sensitivity are highly demanded.

To this end, we herein designed a novel magnetically active AA probe NN-CN-TFFP bearing a nitronyl-nitroxide moiety as an AA-reactive fluorescence quenching group (see **Scheme 2.1a**). As a fluorescence signalling unit, cyanostilbene type π-conjugated backbone was chosen. We have previously reported that molecules with cyanostilbene type backbone formed very stable nanoparticles by self-assembly in aqueous condition.[35, 36]

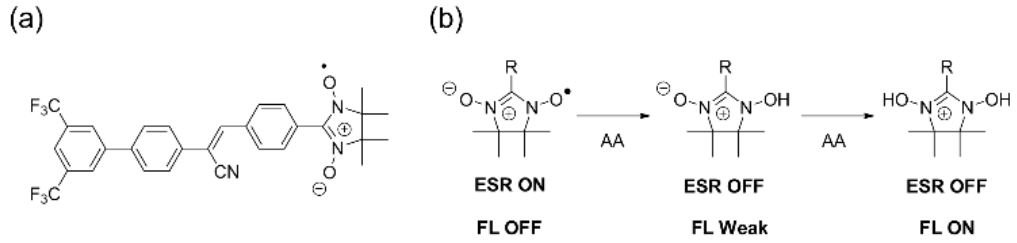

Scheme 2.1. a) Chemical structure of NN-CN-TFFP and **b)** proposed reaction mechanism of NN-CN-TFFP with ascorbic acid and their bimodal responses. FL indicates the fluorescence signal.

2.2. Experimental

Material : NN-CN-TFFP was synthesized through a series of chemical reactions including reduction, Suzuki coupling, Knoevenagel condensation, and oxidation. The probe was fully characterized by ^{1}H NMR, ^{13}C NMR, elemental analysis, MS, and electron spin resonance (ESR) spectroscopy..

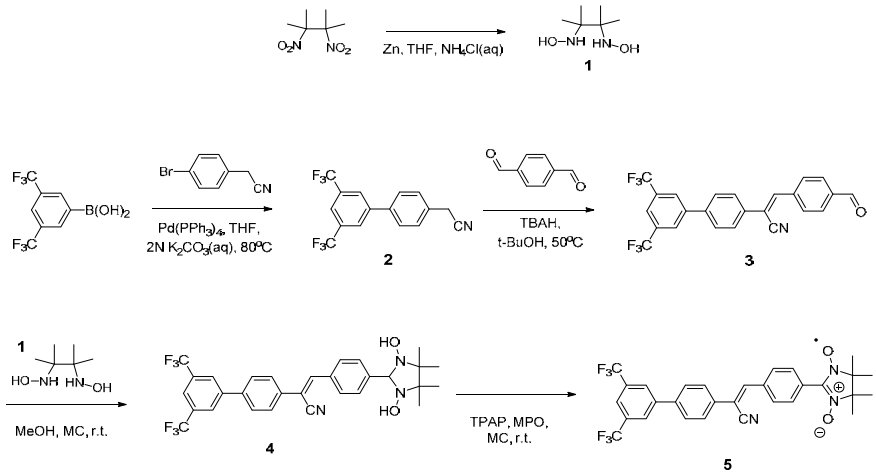

Scheme 2.2. Synthetic route of NN-CN-TFFP.

2.3. Results and discussion

Nitroxides have been reported as a promising reactive unit for AA detection in many previous studies because they are able to quench the excited-state of the covalently linked fluorophore due to their paramagnetic doublet spin.[34] The chemical reduction of the nitroxides by AA would change the paramagnetic spin into a diamagnetic hydroxylamine, and hence turn on the fluorescence

simultaneously with diminished electron spin resonance (ESR) signal.[23, 27, 29] In contrast to the typical nitroxides (*e.g.*, TEMPO), it has been suggested that nitronyl-nitroxides can quench the fluorescence even after losing the doublet spin through photoinduced electron transfer (PET) process due to their imidazole-type structure.[33, 37, 38] Thus, it is expected that the fluorescence of NN-CN-TFFP will be effectively quenched by the cooperative effects of the nitroxide radical and PET from the imidazole structure. Based on our design strategy, we hypothesize that both the sensitivity and detection range of NN-CN-TFFP for AA will be greatly improved as a result of dual-quenching effect and bimodal spectral responses originating from the dual-reactiveness of the nitronyl-nitroxide.

NN-CN-TFFP was synthesized through a series of chemical reactions including reduction, Suzuki coupling, Knoevenagel condensation, and oxidation. The probe was fully characterized by ^{1}H NMR, ^{13}C NMR, elemental analysis, MS, and electron spin resonance (ESR) spectroscopy (see synthetic details and **Scheme 2.2**).

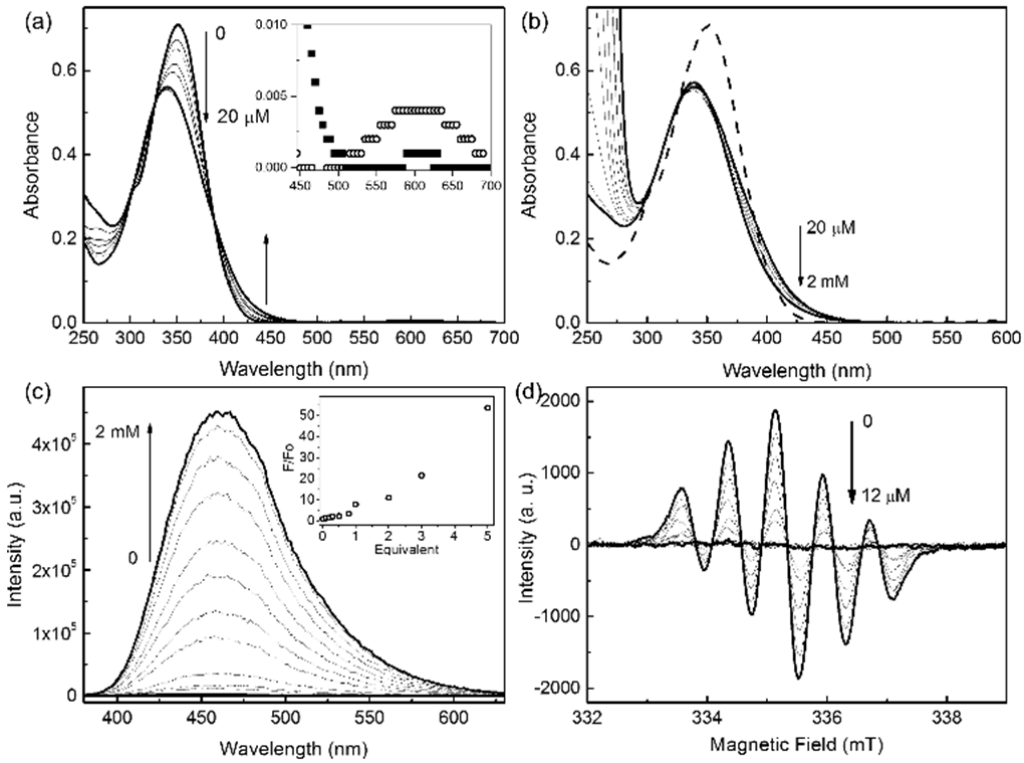

Figure 2.1. Various spectral responses of 20 M NN-CN-TFFP in MeOH solution to increasing concentrations of AA: Changes in absorption spectra upon addition of **a)** 0–20 μM (1 eq.) and **b)** 20

μM (1eq.)–2 mM (100 eq.) AA, and in **c)** fluorescence and **d)** ESR spectra upon addition of 0-2 mM AA. Inset in **a)** presents a magnified absorbance graph of NN-CN-TFFP in the absence (○) and presence (●) of 20 μM AA, respectively. The dashed line in **b)** indicates absorption spectrum of pristine NN-CN-TFFP solution. Inset in **c)** plots the relative fluorescence intensity (F/F_0) versus the equivalent of added AA. F and F_0 are the integrated fluorescence intensities.

First we examined the absorption and fluorescence spectra of the probe in MeOH solution. As shown in **Figure 2. 1a**, two characteristic bands were observed in the absorption spectrum: One is π-π* transition band of the aromatic backbone (ε = 35400 M^{-1} cm^{-1}) at 350 nm and the other is very weak n-π* transition band of the nitronyl-nitroxide moiety (ε = 200 M^{-1} cm^{-1}) at 600 nm,[39] well corresponding with the theoretical results calculated by DFT/TD-DFT method (see **Figure. 2.S1** and **Table 2.S1** in **2.4 supplementary information**). As expected, fluorescence of NN-CN-TFFP was very hard to detect (Φ_{PL} < 0.0001) attributed to efficient fluorescence quenching of the nitronyl-nitroxide moiety. After addition of AA, a significant fluorescence increase was observed with the maximum emission wavelength at 460 nm (**Figure. 2.1c**). The increase of fluorescence intensity reached a maximum of 260-fold (Φ_{PL} = 0.014) when 2 mM of AA is added.

To gain insights into the mechanism of such high fluorescence turn-on, various spectral changes including UV-Vis absorption, fluorescence, and ESR were closely monitored by addition of various concentrations of AA into the probe solution. As shown in **Figure. 2.1a**, upon increasing AA concentration from 2 μM to 20 μM, the characteristic absorption band of NN-CN-TFFP at 350 nm and 600 nm gradually decreased whilst a new band at around 430 nm increased. However, it was observed that the isosbestic points were not kept constant at 325 nm and 380 nm but began to move when more than 0.5 eq. of AA (10 μM) was added (see **Figure. 2.S2** in **2.4 supplementary information**). In addition, further increase of AA concentration generated a new trend of the absorption spectra change. After addition of more than 20 μM of AA, the absorption bands at around 400 nm started to decrease reversely (see **Figure. 2.1b**), implying that two different reaction occurs between NN-CN-TFFP and AA depending on AA concentration.

On the other hand, the fluorescence intensity of the probe gradually increased upon AA addition. It should be noted that the fluorescence intensity barely increased until the AA concentration reached to

10 μM which is 0.5 eq. concentration to that of NN-CN-TFFP (**Figure. 2.1c** and **Figure. 2.S2** in **2.4 supplementary information**). But, after exceeding that concentration, the fluorescence intensity started to increase drastically.

We also investigated changes in ESR spectrum of NN-CN-TFFP upon AA addition. The nitrogen atom possessing spin I = 1 interacts with an unpaired electron (*i.e.*, radical), resulting in splitting the electron resonance line of a molecule into three equally intense lines.[40, 41] Due to the two equivalent nitrogen nuclei of the imidazole moiety of NN-CN-TFFP, five lines (g = 2.0075, $|a_N|$ = 0.764 mT) were clearly observed with an intensity ratio of 1:2:3:2:1 as shown in **Figure. 2.1d**, which is consistent with the typical ESR spectrum of nitronyl-nitroxides.[42] As expected, the ESR signal gradually diminished upon AA addition and completely disappeared at 12 μM where the AA concentration is just over 0.5 eq. of the probe concentration.

Taken all together, it is deduced that two different reactions took place sequentially upon AA addition (see Scheme 1b). First, from 2 μM to 12 μM of AA addition range, it was brought about the reduction of nitronyl-nitroxide moiety of the probe. AA is a mild reducing agent and typically reacts with a nitroxide to yield a diamagnetic hydroxylamine.[43] The linearly decreased ESR signal and the vanished n-π* absorption band at 600 nm provided corroborative evidence for the occurrence of reduction. Because AA is usually oxidized with the loss of two electrons to form dehydroascorbic acid, it is expected that the addition of 0.5 eq. AA to NN-CN-TFFP solution is enough to reduce all of the nitroxide unit into hydroxylamines.[44] But, the ESR spectrum with addition of 10 μM AA still exhibited a weak signal and 0.6 eq. of AA is needed to eliminate the signal completely. Considering together with the shift of isosbestic points in the absorption spectra, it is reasonable to infer that another kind of reaction started to occur subsequently. Although all radicals are reduced by AA, it is noteworthy that the fluorescence intensity of probe remains still very low. It indicates that additional fluorescence quenching site still subsists.

The subsequent reaction is most likely the protonation of the probe. It was reported that treatment of the nitronyl-nitroxides with acids led to protonation of the NO group.[32, 37, 38, 45] AA is also acidic (pKa_1 = 4.1 and pKa_2 = 11.97) and would protonate the NO group of NN-CN-TFFP. With addition of AA

from 20 μM to 2 mM, it is observed that the absorbance and the fluorescence of probe gradually changed (**Figure. 2.1b and c**). DFT/TD-DFT results also revealed that the protonation of NO moiety leads to the decrease of absorption at longer wavelength (see **Figure. 2.S1 and Table S1** in **2.4 supplementary information**), consistent with the experimental results shown in **Figure. 2.1**. It should be noted that the fluorescence of the probe was significantly enhanced, indicating that the fluorescence quenching sites are fully arrested by the protonation.

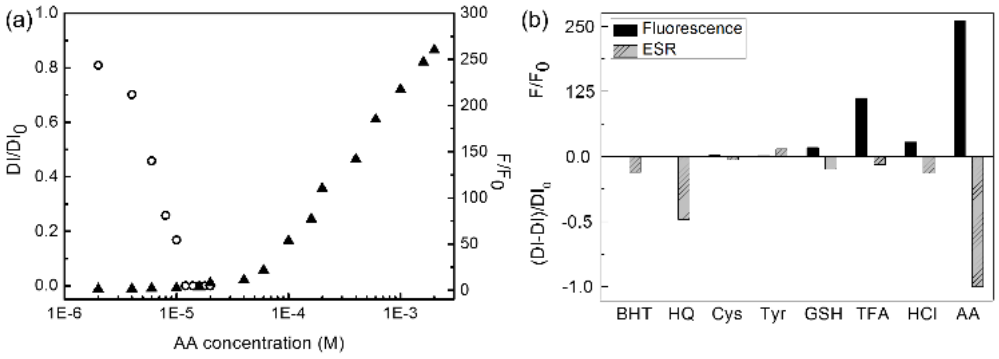

Figure 2.2. Plots of the relative fluorescence intensity (F/F_0) and ESR intensity (DI/DI_0) of 20 μM NN-CN-TFFP in MeOH solution versus **a)** the concentration of AA and **b)** 2 mM of various antioxidants and acids. F and F_0 are the integrated fluorescence intensities, and DI and DI_0 are the double integrated ESR intensities of NN-CN-TFFP solution in the presence and absence of AA, respectively.

To further evidence the protonation effect on the fluorescence turn-on, we added excessive amount of trifluoroacetic acid (TFA) and hydrochloric acid (HCl) to NN-CN-TFFP solution, respectively. It was observed that the addition of the strong acids led to 117-fold and 29-fold increases of the fluorescence intensity for TFA and HCl, respectively, as shown in **Figure. 2.2b**, while no significant change was observed in their ESR spectra (see **Figure. 2.2b** and **Figure. 2.S3** in **2.4 supplementary information**). In contrast, addition of hydroxyquinone (HQ), a well-known reducing agent, induced negligible increase of the fluorescence intensity even though the ESR signal decreased by half (see **Figure. 2.2b** and **Figure. 2.S3** in **2.4 supplementary information**). These experiments clearly suggest that NN-CN-TFFP has two fluorescence quenching group, NO (*i.e.*, imidazole structure) and NO• (*i.e.*, nitroxide radical), among which the former is more effective.

To gain detailed information about the sensitivity of NN-CN-TFFP to AA, we analysed the fluorescence intensity changes upon AA addition. It is revealed that the relative fluorescence intensity was linearly related to the AA concentration from 10 μM to 0.2 mM (F/F_0 = 0.547 [AA]/ μM – 4.80 where R^2 = 0.982, see ESI **Figure. 2.S4a**). Specifically the limit of detection (LOD) was found to be as low as 13.6 μM. In addition, NN-CN-TFFP exhibited a linear response toward logarithm of AA concentration from 0.1 mM to 2 mM, and the linear equation was F/F_0 = 154 log [AA] + 677 with R^2 = 0.991 (see **Figure 2.2a** and ESI **Figure. 2.S4b**). It must also be noted that the ESR measurements could detect AA from 2 μM to 12 μM where the concentration is below the LOD of fluorescence measurements (see **Figure. 2.2a** and ESI **Figure. 2.S5**). The relative ESR intensity showed good linear relationship toward AA concentration (DI/DI_0 = –0.844 [AA]/ μM – 0.991 where R2 = 0.989) with a 0.937 μM of LOD.

In order to evaluate the selectivity, NN-CN-TFFP solution was treated with excess amounts of various antioxidants (see **Figure. 2.2b**). Cysteine (Cys), Tyrosol (Tyr), and Gluotathione (GSH) exhibited no significant changes in both fluorescence and ESR spectra of the solution. HQ and butylated hydroxyl toluene (BHT) decreased the ESR intensity but affected no fluorescence intensity. It is worth noting that the strong acids such as TFA and HCl turned on the fluorescence of NN-CN-TFFP solution, however, one can easily distinguish AA from the acids by the ESR signal as described above. These results clearly indicate that the dual-reactiveness and dual-quenching of nitronyl-nitroxide group provides not only high sensitivity with a wide detection range but also high selectivity.

Finally, we examined whether NN-CN-TFFP can detect AA in aqueous condition for practical uses. As shown in **Figure. 2.3a**, the probe molecules could form 100 nm-sized nanoparticles in aqueous condition (water/THF = 7:3 in vol %) by self-assembly without any surfactants. ESR spectrum with clear five line pattern indicates that the nitronyl-nitroxide radicals were completely preserved in the nanoparticles (see **Figure. 2.3b**). Similarly to the methanol solution, upon addition of AA, NN-CN-TFFP nanoparticles showed bimodal responses in fluorescence and ESR spectra. With increasing AA concentration, ESR signal of the nanoparticles gradually decreased. But, in sharp contrast to the methanol solution, the nitroxide moiety remained unreacted until the AA concentration reached to 0.4

mM. The fluorescence intensity of nanoparticles also showed significant increases after 0.4 mM of AA was added. This is attributable to that NN-CN-TFFP molecules close to the centre of nanoparticles have significantly less chance to react with AA before the nitronyl-nitroxide moieties near the nanoparticle surfaces are completely reduced and protonated by AA. Therefore, more AA molecules are needed to diminish the ESR and to recover the fluorescence signal of nanoparticles than those of methanol solution.

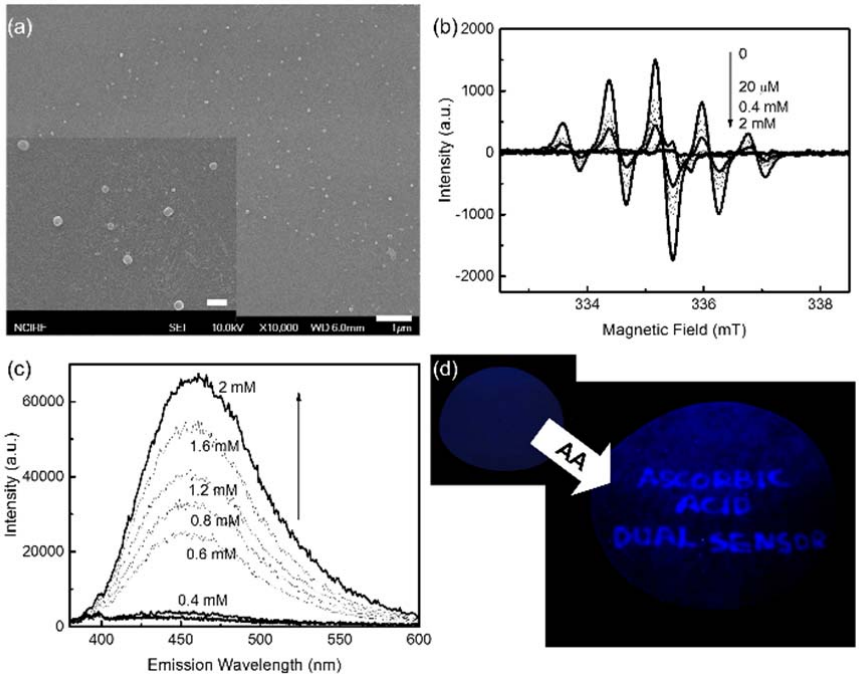

Figure 2.3. a) FE-SEM images of NN-CN-TFFP nanoparticles. Scale bar in the inset figure indicates 200 nm. **b)** ESR and **c)** fluorescence responses of NN-CN-TFFP nanoparticles (20 μM in water/THF = 7:3 in vol %) upon addition of AA. **d)** Fluorescence photoimages of the fluorescent paper sensor for AA under 365 nm handheld UV lamp before (left) and after (right) writing letters with AA solution as ink.

In summary, we could demonstrate a novel fluorescent AA probe bearing nitronyl-nitroxide as an AA-reactive unit. The fluorescence enhancement of probe by AA addition was as high as 260-fold in methanol solution. The probe could detect AA from as low as 0.937 μM up to 2 mM, which satisfies the needs in various analytic samples, and showed excellent selectivity over various antioxidants and acids. The high selectivity and sensitivity with a broad detection range of the probe originated from

the dual-reactiveness of dual-quenching group nitronyl-nitroxide. Furthermore, we prepared nanoparticles and a sensor paper using the probe, and examined AA detection capabilities in aqueous condition and solid-state, respectively, for practical applications.

2.4. Spplementary information

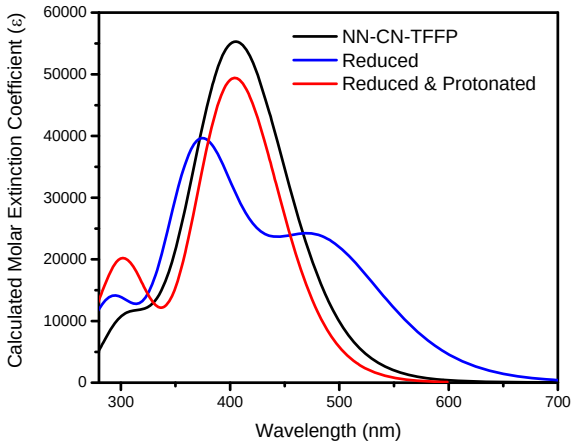

Figure 2.S1. Calculated absorption spectra of NN-CN-TFFP in MeOH.

Name	Transition	Energy	Oscillator Strength (*f*)	Orbitals (Expansion Coefficient)	Character
NN-CN-TFFP (doublet, neutral)	Excited-State 1	1.93 eV (643.68 nm)	0.0004	HOMOa → LUMOa (0.86268) HOMOa → LUMOa+1 (0.14148) HOMOa → LUMOa+2 (-0.19650)	n-π*
	Excited-State 5	2.94 eV (421.48 nm)	0.5821	HOMOa-2 → LUMOa (0.27517) HOMOa-1 → LUMOa (-0.47586) HOMOa-1 → LUMOa+1 (0.20451)	π- π *
	Excited-State 7	3.11 eV (398.38 nm)	0.6706	HOMOa-8 → LUMOa+2 (0.12609) HOMOa-2 → LUMOa (-0.32292) HOMOa-2 → LUMOa+1 (0.12434) HOMOa-1 → LUMOa (-0.42893) HOMOa-1 → LUMOa+1 (-0.29574)	π - π *
Reduced (singlet, neutral)	Excited-State 1	2.57 eV (482.14 nm)	0.5598	HOMO → LUMO (0.70348)	π - π *
	Excited-state 2	3.31 eV	0.9422	HOMO-1 → LUMO (0.69987)	π - π *

		(374.04 nm)			
Reduced & Protonated (singlet, cationic)	Excited-State 1	3.07 eV (404.45 nm)	1.2189	HOMO → LUMO (0.70409)	π - π *

Table 2.S1. Calculated energies, oscillator strength, orbitals, and character of absorption transition of NN-CN-TFFP in MeOH.

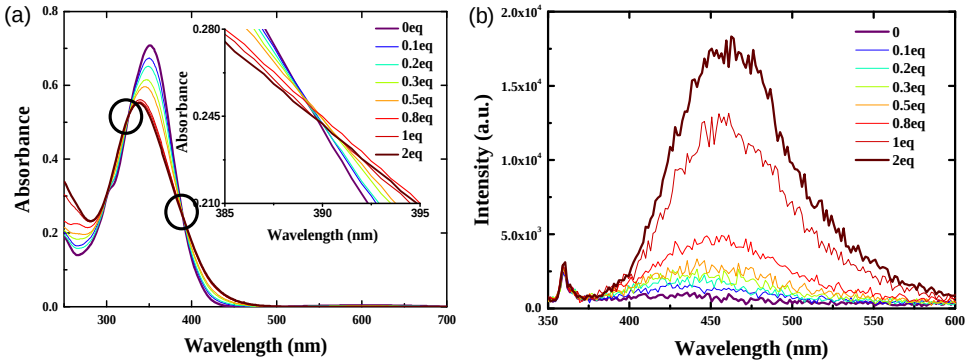

Figure 2.S2. Absorption and photoluminescence spectra changes of 20 M NN-CN-TFFP in MeOH solution upon addition of 0–40 M AA.

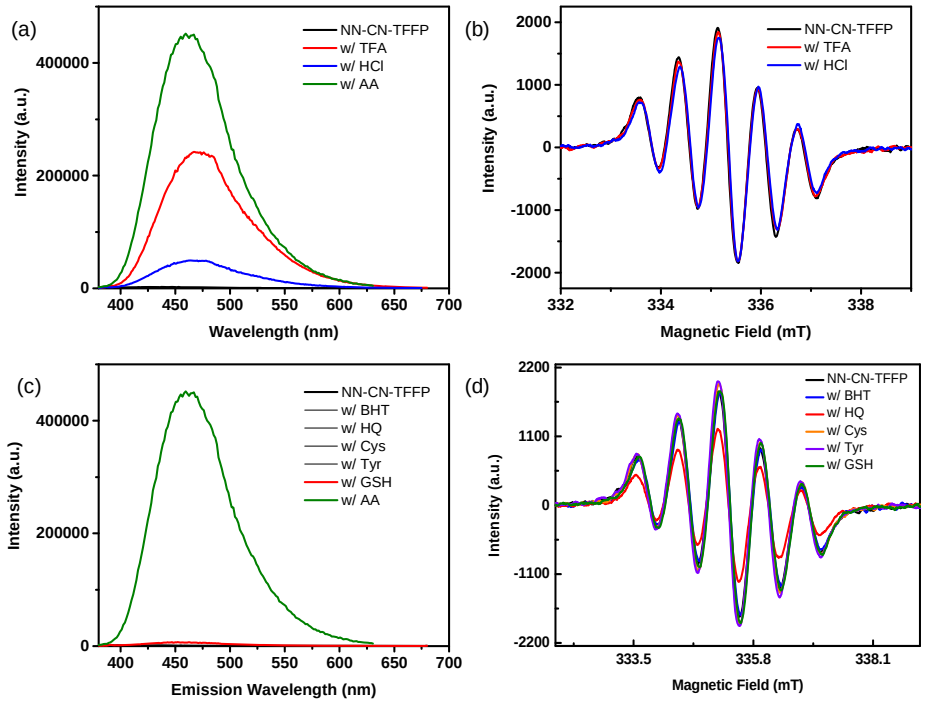

Figure 2.S3. a) Photoluminescence and **b)** ESR spectra of NN-CN-TFFP with addition of various acids. **c)** Photoluminescence and **d)** ESR spectra of NN-CN-TFFP with addition of various antioxidants.

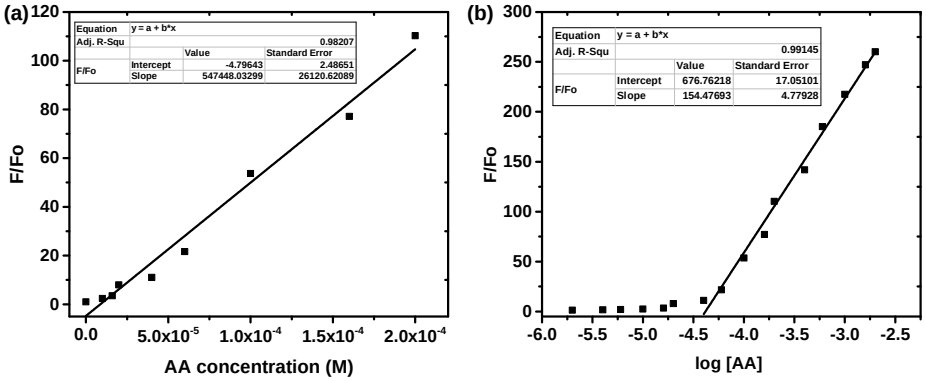

Figure 2.S4. Linear relationship between the relative fluorescence intensity (F/F_0) and AA concentration **a)** from 10 M to 0.2 mM and **b)** from 0.1 mM to 2 mM.

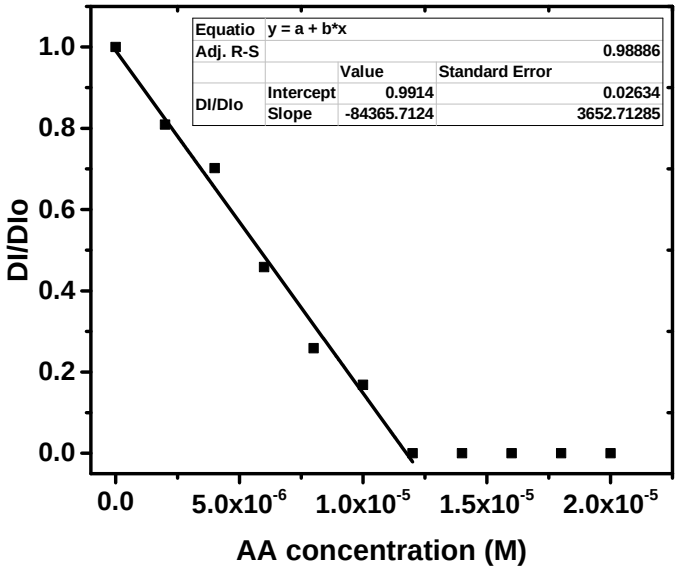

Figure 2.S5. A Linear relationship between the relative double integratged ESR intensity (DI/DI_0) and AA concentration.

2.5. References

[1] B. Peterkofsky and S. Udenfriend, *Proc. Natl. Acad. Sci. U. S. A.*, 1965, **53**, 335.
[2] O. Arrigoni and M. C. De Tullio, *BBA Gen. Subjects*, 2002, **1569**, 1.
[3] G. F. Combs Jr., in *The Vitamins: Fundamental Aspects in Nutrition and Health*, Academic Press, 4th edn., 2012.
[4] S. P. Sood, L. E. Sartori, D. P. Wittmer and W. G. Haney, *Anal. Chem.*, 1976, **48**, 796.
[5] A. M. Pisoschi, A. F. Danet and S. Kalinowski, *J. Autom. Method. Manag.*, 2008, **2008**, 937651.
[6] Q. Chen, M. G. Espey, M. C. Krishna, J. B. Mitchell, C. P. Corpe, G. R. Buettner, E. Shacter and M. Levine, *Proc. Natl. Acad. Sci. U. S. A.*, 2005, **102**, 13604.
[7] J. A. Jackson, K. Wong, C. Krier, H. D. Riordan, *J. Orthomol. Med.*, 2005, **20**, 3.
[8] W.-S. Kim, R. L. Dahlgren, L. L. Moroz and J. V. Sweedler, *Anal. Chem.*, 2002, **74**, 5614.
[9] A. Bossi, S. A. Piletsky, E. V. Piletska, P. G. Righetti and A. P. F. Turner, *Anal. Chem.*, 2000, **72**, 4296.
[10] K. Güçlü, K. Sözgen, E. Tütem, M. Özyürek and R. Apak, *Talanta*, 2005, **65**, 1226.
[11] V. Gökmen, N. Kahraman, N. Demir and J. Acar, *J. Chromatogra. A*, 2000, **881**, 309.
[12] M. Zhang, K. Liu, L. Xiang, Y. Lin, L. Su and L. Mao, *Anal. Chem.*, 2007, **79**, 6559.
[13] P. Janda, J. Weber, L. Dunsch and A. B. P. Lever, *Anal. Chem.*, 1996, **68**, 960.
[14] A. P. Demchenko, in *Introduction to Fluorescence Sensing*, Springer, 2009.
[15] Y. J. Chen and X. P. Yan, *Small*, 2009, **5**, 2012.
[16] W. Zhai, C. Wang, P. Yu, Y. Wang and L. Mao, *Anal. Chem.*, 2014, **86**, 12206.
[17] M. Zheng, Z. Xie, D. Qu, D. Li, P. Du, X. Jing and Z. Sun, *ACS Appl. Mater. Interfaces*, 2013, **5**, 13242.
[18] X. Wang, P. Wu, X. Hou and Y. Lv, *Analyst*, 2013, **138**, 229.
[19] H. W. Park, S. M. Alam, S. H. Lee, M. M. Karim, S. M. Wabaidur, M. Kang and J. H. Choi, *Luminescence*, 2009, **24**, 367.
[20] N. Malashikhina and V. Pavlov, *Biosens. Bioelectron.*, 2012, **33**, 241.
[21] C. Kong, D. W. Li, Y. Li, R. Partovi-Nia, T. D. James, Y. T. Long and H. Tian, *Analyst*, 2012, **137**, 1094.
[22] L. Cao, Q. Wu, Q. Li, S. Shao and Y. Guo, *New J. Chem.*, 2013, **37**, 2991.
[23] W. Chen, X. Wang, X. Tu, D. Pei, Y. Zhao and X. Guo, *Small*, 2008, **4**, 759.
[24] K. Ishii, K. Kubo, T. Sakurada, K. Komori and Y. Sakai, *Chem. Commun.*, 2011, **47**, 4932.
[25] F. Lin, D. Pei, W. He, Z. Huang, Y. Huang and X. Guo, *J. Mater. Chem.*, 2012, **22**, 11801.
[26] C.-P. Liu, T.-H. Wu, C.-Y. Liu, H.-J. Cheng and S.-Y. Lin, *J. Mater. Chem. B*, 2015, **3**, 191.
[27] D. Pei, J. Hong, F. Lin, Z. Shi, Z. Chen, H. Nie and X. Guo, *Chem. Commun.*, 2011, **47**, 9492.
[28] Y. L. Tang, F. He, M. H. Yu, S. Wang, Y. L. Li and D. B. Zhu, *Chem. Mater.*, 2006, **18**, 3605.
[29] T. Yang, B. Zheng, H. Liang, Y. Wan, J. Du and D. Xiao, *Talanta*, 2015, **132**, 191.
[30] N. B. Yapici, S. Jockusch, A. Moscatelli, S. R. Mandalapu, Y. Itagaki, D. K. Bates, S. Wiseman, K. M. Gibson, N. J. Turro and L. R. Bi, *Org. Lett.*, 2012, **14**, 50.
[31] B. Bognár, J. Jekő, T. Kálai and K. Hideg, *Dyes Pigments*, 2010, **87**, 218.
[32] Y. B. Borozdina, V. Kamm, F. Laquai and M. Baumgarten, *J. Mater. Chem.*, 2012, **22**, 13260.
[33] N. Medvedeva, V. V. Martin, A. L. Weis and G. I. Likhtenshten, *J. Photochem. Photobiol. A: Chem.*, 2004, **163**, 45.
[34] G. I. Likhtenstein, K. Ishii and S. Nakatsuji, *Photochem. Photobiol.*, 2007, **83**, 871.
[35] B.-K. An, S.-K. Kwon, S.-D. Jung and S. Y. Park, *J. Am. Chem. Soc.*, 2002, **124**, 14410.
[36] S. Shin, S. H. Gihm, C. R. Park, S. Kim and S. Y. Park, *Chem. Mater.*, 2013, **25**, 3288.
[37] H. Wang, L. Jing, Z. Xiang, P. Liu, X. Sun and R. Jiang, *Bull. Chem. Soc. Japan*, 2011, **84**, 341.
[38] H. Wang, D. Zhang, X. Guo, L. Zhu, Z. Shuai and D. Zhu, *Chem. Commun.*, 2004, 670.
[39] E. F. Ullman, L. Call and J. H. Osiecki, *J. Org. Chem.*, 1970, **35**, 3623.
[40] A. R. Forrester, J. M. Hay, R. H. Thomson, in *Organic Chemistry of Stable Free Radicals*, Academic Press, London, 1968.
[41] J. E. Wertz, J. R. Bolton, in *Electron Spin Resonance, Elementary Theory and Practical Applications*, Chapman and Hall, New York, 1986.

[42] E. F. Ullman, J. H. Osiecki, D. G. B. Boocock and R. Darcy, *J. Am. Chem. Soc.*, 1972, **94**, 7049-7059.
[43] E. Breuer, H. G. Aurich, A. Nielsen, Z. Rappoport, in *Nitrones, Nitronates and Nitroxides*, John Wiley & Sons, 1989.
[44] Y. H. P. Hsieh and Y. P. Hsieh, *J. Agr. Food. Chem.*, 2000, **48**, 1569.
[45] J. H. Osiecki and E. F. Ullman, *J. Am. Chem. Soc.*, 1968, **90**, 1078.

Chapter 3. Collaboration works

3.1. Optically tunable Seebeck effect from intramolecular proton-transfer materials.

HPI-Cbz has shown excited state induced proton transfer (ESIPT) behavior [1]. HPI-Cbz was synthesized in the Park laboratory and fabricated as devices for measuring Seebeck effect in Hu laboratory. **Scheme 3.1** showed synthetic route and molecular structure of HPI-Cbz[1]. Large Seebeck coefficients of 428 μV/K and 390 μV/K were observed from HPI-Cbz based thin-film devices at 60 ^{o}C when proton-transfer was induced by the photoexcitation of a 325 nm laser with an intensity of 12 mW/cm^2 and 6 mW/cm^2 respectively (**Figure 3.1**). The Seebeck coefficient enhancement by the induced intramolecular charge transfer can be attributed to the enhanced polarization difference between high- and low-temperature surface and enhanced temperature-dependent electrical polarization. Detailed explanation will be described in Hu's reports.

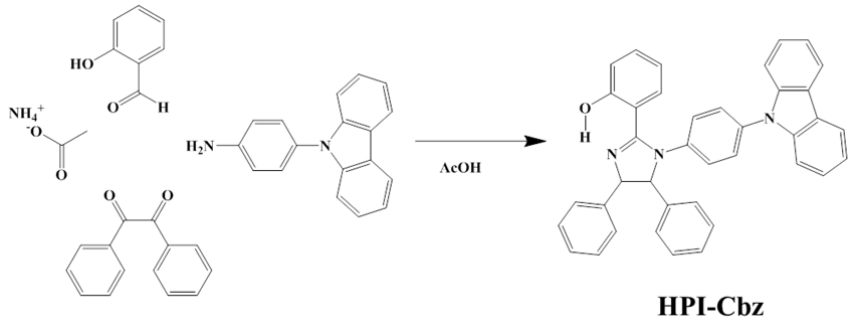

Scheme 3.1. Synthetic route of HPI-Cbz

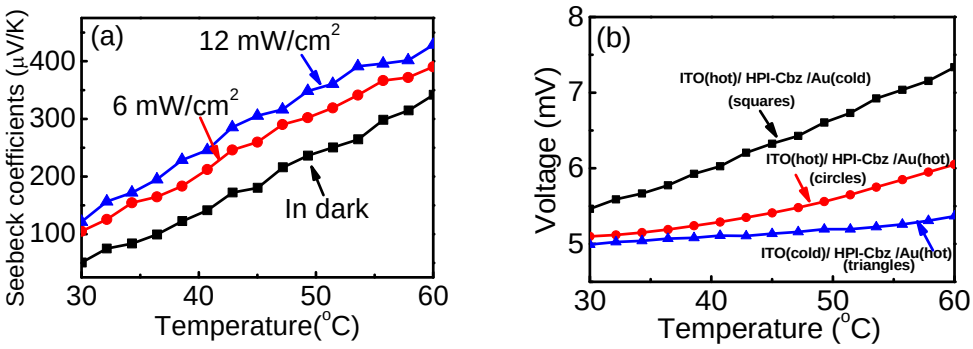

Figure 3.1 (a) Seebeck coefficients measured from ITO/HPI-Cbz/Au device in dark conditions and under photoexcitation of 12 mW/cm^2 and 6 mW/cm^2 at 325 nm. (b) Overall voltages of the ITO/HPI-Cbz/Au device with forward, reverse and negligible temperature gradients at different temperatures.

3.2. Materials preparation

We supplied CN-TFMBPPE to Bin Hu group for (i) magnetic field effects of photoluminescence and (ii) magnetic field effects of light scattering in organo-gel. **Scheme 3.2** showed synthetic route and molecular structure of CN-TFMBPPE[2].

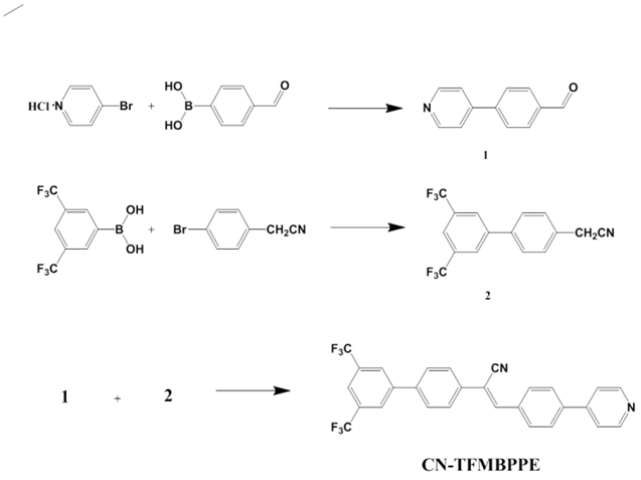

Scheme 3.2. Synthetic route of CN-TFMBPPE

3.3. References

1 S. Park, J. Seo, S. H. Kim, S. Y. Park, Advanced Functional Materials 2008, 18, 726.

2 J. Seo, J. W. Chung, E.-H. Jo, S. Y. Park, Chemical Communications 2008, 2794.

Publications works

a) Chapter 1 : manuscripts will soon be submitted to peer-reviewed journals.

Jin Hong Kim, Song-Toan Pham, Hirokazu Tada, and Soo Young Park, Tuning the organic magnetoresistance in single layer ambipolar transistors by controlling minority charge carrier injection

b) Chapter 2 : manuscripts will soon be submitted to peer-reviewed journals.

Haerim Nam, Ji Eon Kwon, Jangwon Seo, Seunghoon Shin, Sehoon Kim, and Soo Yong Park, Highly sensitive and selective fluorescent probe for ascorbic acid with a broad detection range through dual-quenching and bimodal action of nitronyl-nitroxide

c) Chapter 3 : published in peer-reviewed journals

Dehua Hu, Qing Liu, Jeremy Tisdale, Haerim Nam, Soo Young Park, Hsin Wang, Augustine Urbas, and Bin Hu, Optically tunable Seebeck effect from intramolecular proton-transfer materials in organic vertical thin-film thermoelectric device, Organic Electronics, Volume 26, November 2015, Pages 117-120

(**Note**. Although the corresponding author didn't cite our grant number of this project, the material (HPI-Cbz) was supplied by our group as the main mission of this collaboration project.)